STABILIZATION OF EXTERNAL LOADS IN HIGH SPEED FLIGHT USING AN ACTIVE CARGO HOOK

Jacob Enciu, Ajay Singh, Joseph F. Horn
Department of Aerospace Engineering, The Pennsylvania State University,
University Park, PA 16802

Abstract

The use of an active cargo hook for stabilizing external loads during high speed flight is demonstrated in simulation. A CONEX cargo container with two rear mounted stabilization fins is used as the subject load. Significant nonlinearities in the dynamics of the external load result in multiple equilibria and limit cycle oscillations. A full state feedback linear quadratic controller is developed assuming an isolated load in wind tunnel model and shown to be successful in stabilizing the originally unstable load at a target airspeed of 100 kt. The design is then completed to cover the target carriage envelope from hover to high speed flight. Simulations of a coupled system incorporating a UH-60 Black Hawk helicopter with an actuated cargo hook and the external load show that the controller is successful in providing system stability throughout the target flight speed envelope.

NOTATION

$\mathbf{A},\mathbf{B},\mathbf{C},\mathbf{D}$	=	Matrices in system linear model
C_S	=	cable damping coefficient
$\mathbf{F}_S$	=	cable tension force
f_Q, f_R	=	scaling ratio functions
$\mathbf{G}_{CH}$	=	Cargo hook actuator model
$\mathbf{K}$	=	gain matrix
K_S	=	cable stiffness
l	=	loaded cable length
$\mathbf{P}$	=	Solution of Riccati equation
p,q,r	=	roll, pitch and yaw rates
$\mathbf{Q}$	=	state weight matrix
$\mathbf{R}$	=	Control weight matrix
t	=	time
$\mathbf{u}$	=	control command vector
u,v,w	=	inertial velocity components
V	=	airspeed
X_A, X_B, X_C, X_P	=	lateral and longitudinal stick, collective, pedals
x,y,z	=	longitudinal, lateral and vertical position
$\mathbf{x}$	=	state vector
$\beta_0, \beta_{1S}, \beta_{1C}$	=	main rotor flapping angles
$\Delta r_{CH}, \Delta x_{CH}, \Delta y_{CH}$	=	absolute, longitudinal and lateral cargo hook stroke
Δl	=	cable stretch
$\boldsymbol{\delta}$	=	Vector of pilot control commands
$\lambda_0, \lambda_{1S}, \lambda_{1C}$	=	dynamic inflow components
χ	=	trajectory heading angle
ψ,θ,ϕ	=	yaw, pitch and roll angles
ω_A	=	actuator frequency
ω_F	=	low pass filter frequency
$(\,)_A$	=	actuated system
$(\,)_F$	=	fuselage
$(\,)_H$	=	helicopter
$(\,)_L$	=	load
$(\,)_{N,E,D}$	=	north, east, down
$(\,)_R$	=	main rotor
$(\,)_W$	=	Wind tunnel
$\dot{\square}$	=	time rate of change
$\hat{\square}$	=	unit vector

1. INTRODUCTION

External carriage of underslung loads by rotorcraft enables efficient transportation of large and heavy payloads to their target locations. However, the underslung load adds dynamic modes that in many cases degrade the stability of the coupled helicopter-slung load system and its handling qualities. This leads to limiting of the maximum certified safe carriage envelope for many external loads. Box-like loads (cargo containers), plate-like loads and different types of military loads were shown to be prone to instabilities during single point carriage [1]. Difficult loads are currently limited to airspeeds below 60 knots. This impacts the operational efficiency of slung load missions and increases the risk to the flight crew during operation in hostile zones. Therefore, a

key objective of slung-load research and development is load stabilization during forward flight. The introduction of tilt-rotors and other high speed rotary aircraft configurations in the near future will further expand the attainable flight speeds with external loads. This will dictate a need for the development of means for efficient stabilization methods for external loads during high speed flight.

Different techniques for passive and active stabilization of slung loads were studied in the past by various researchers [2-10]. A different approach for the avoidance of slung load instabilities during flight involved the use of a flight director that provided pilots with guidance cues for damping the load pendulum modes [11-14]. None of these efforts have matured into an operational system.

In recent years, stabilization of external loads was demonstrated by a collaborative research by Technion University and the US Army. Stabilization methods included both passive stabilization using rear mounted fixed fins [15] and active rotational stabilization using controlled anemometric cups [16]. Both methods were demonstrated in flight and produced an extended carriage envelope of ~ 120 kt for box-like loads. While successful in providing system stability, the implementation of these methods in an operational scenario will be complicated by the logistics involved in preparing the loads for flight and retrieving the stabilization equipment post mission. Further, the modification of the load to include the stabilization hardware increases the load weight and drag and leads to performance penalties.

Another issue with external cargo missions is the high pilot workload required during load placement. Precise placement of the load requires high gain control by the pilot. The coupling between the load pendulum motion and the helicopter dynamics produces degraded handling qualities and increases pilot workload. Active load stabilization techniques were studied as means for damping of the load pendulum motions near hover. Load stabilization at hover and low speed flight using cable angle feedback (CAF) was demonstrated by Ivler [17]. The use of CAF improved the load damping by trading between position hold performance and load stability. Krishnamurthi and Horn [18] investigated cable angle feedback into the primary flight control system and showed that the use of relative cable angles measurements and a lagged cable angle compensator (LCAF) provided good load stabilization in hover and low speed flight.

An active cargo hook (ACH) using the LCAF control law was recently flight demonstrated by the Boeing Company [19]. The system was flight tested on Boeing's H-6 flying test bed, utilizing a load to mass (LMR) ratio of 0.09 and a cable length of 25 ft. Results showed a significant increase in load damping during low speeds and reduced pilot workload during load placement.

A preliminary study was later conducted by the Vertical Lift Research Center of Excellence (VLRCOE) at Penn State University for studying the feasibility of using an ACH for load stabilization during high speed flight. The study used a formerly validated dynamic model of a CONEX cargo container with two rear mounted fins, mounted in a wind tunnel [20]. A simple roll angle feedback controller was designed to drive the ACH. Simulations were used to investigate the controller efficiency in stabilizing the load in a target airspeed of 100 kt. The results showed that the ACH was able to provide a damping ratio of 0.05, similar to to the values obtained in Ref. [19] for hover. Results also demonstrated that the controller should always be engaged for maximum effectiveness. Switching the controller only after encountering instabilities failed in some cases to provide positive damping due to ACH saturation.

A research program for the development of stabilization methods of external loads during high speed flight was recently initiated by the USARMY-AMRDEC. The research will be performed collaboratively by researchers from Penn State University and the Technion and will include the development of active stabilization controllers for external load carriage and their validation by real-time piloted simulations and hardware in the loop wind tunnel tests.

This paper describes the development of a full state feedback linear-quadratic regulator (LQR) controller for an active cargo hook, to provide external load stability during high speed flight. Although the main focus is on high speed flight, controller design was accomplished for all airspeeds (from hover to the maximum target airspeed). The outline of the paper is as follows: first, the dynamic models of the isolated external load, helicopter, and coupled helicopter-load system are described. Then, the nonlinear dynamical characteristics of the isolated load ("load in a wind tunnel") are briefly introduced. Next, the design of the LQR controller of the active cargo hook is presented following by simulation results of the controller performance for various airspeeds. Simulation results for the coupled helicopter-slung load system utilizing the ACH are then brought for validation of the controller performance when the load is carried by a helicopter. Finally, the main conclusions of this effort are summarized.

2. DYNAMIC MODELING

The system is comprised of a UH-60 Black Hawk utility helicopter carrying a CONEX cargo container with rear mounted fins. Four 18.7 ft sling cables connect the cargo hook of the helicopter to the four corners on the upper surface of the container. Figure

1 shows the system in flight test by the USARMY Aeroflightdynamics Directoarte [15].

Fig. 1. Test helicopter carrying the fins-stabilized CONEX cargo container [15]

2.1. External Load Model

The carried slung load is an 8ft x 6ft x 6ft CONEX cargo container, fitted with two rear mounted fins. The fins are inclined at 33 deg relative to the box side faces, trailing edge out. The load total weight is 2489 lb, which is representative of an empty container plus the four sling cables. As this particular load was used extensively in research activities describes earlier, its dynamic model has been thoroughly validated in a series of wind tunnel tests and flight tests. For the current study, the load center of gravity was set 0.3 ft aft of the CONEX geometric center in order to create an instability at the target airspeed of 100 kt.

The aerodynamic model of the fins stabilized load uses static aerodynamic forces and moments coefficients measured in the wind tunnel for the complete load (fins included). These coefficients are augmented by a theoretical calculation to include the fins quasi-steady damping effect (due to the arm between the fins and the load center of gravity). This procedure for predicting the added aerodynamic contribution of the fins due to load angular rates was found to provide satisfactory agreement with dynamic wind tunnel tests (see Ref. [21] for details). For the studied configuration, it was assumed that the load was connected to the helicopter cargo hook by a swivel, which enabled free yaw rotations of the load with a negligible resisting friction moment.

The load equations of motion are implemented as a state space model with the state vector being comprised of the angular rates, Euler angles, inertial velocities and center of gravity position:

$$\mathbf{x_L} = \{u_L, v_L, w_L, \psi_L, \theta_L, \phi_L, p_L, q_L, r_L, x_N, y_E, z_D\} \quad (1)$$

The angular rates and inertial velocities are given in a load fixed coordinate system (L) located at the center of gravity, with the x axis pointing forward, y axis pointing right and z axis pointing down. The position vector is given in an earth fixed NED inertial system (E), with the x axis pointing to the north, y axis pointing to the south, and z axis pointing down. The transformation from this earth fixed coordinate system to the load fixed coordinate system follows the conventional "321" order of Euler angles rotation:

yaw (ψ_L) $\rightarrow$ pitch (θ_L) $\rightarrow$ roll (ϕ_L).

2.2. Sling Cables Model

Four identical sling cables of 18.7 ft length are connecting the upper surface corners of the load to the helicopter cargo hook. Each cable is modeled as a linear spring and damper combination, presumed to carry only a tension force. It is assumed that the cables do not carry compression forces or bending and torsion moments. The tension force in the i^{th} cable is calculated from the cable stretch, Δl_i, and its rate of change, and is directed along the cable unit length vector, $\hat{\mathbf{l}}_i$:

$$\mathbf{F}_{S,i} = \max(K_{S,i} \cdot \Delta\mathbf{l}_i + C_{S,i}(\Delta\dot{l}), 0) \cdot \hat{\mathbf{l}}_i \quad (2.a)$$

Where:

$$\hat{\mathbf{l}}_i = \frac{\mathbf{l}_i}{|\mathbf{l}_i|} \quad (2.b)$$

The cable vectors are calculated from the positions of the helicopter cargo hook and the four attachment points on the load upper surface. These, in turn, depend on the load position, attitude and geometric properties. Cable directions are defined positive for vectors originating from the cargo hook and pointing into the load attachment point. Stiffness and damping values of 9645 lb/ft and 30.3 lb·sec/ft were used for $K_{S,i}$ and $C_{S,i}$, respectively.

2.3. Helicopter Model

A utility helicopter model of a UH-60 Black Hawk is used in the current research. The helicopter nonlinear model is largely based on the GENHEL engineering simulation of the UH-60 helicopter [22]. The main rotor model employed is simplified as compared to the original simulation of Ref. [22]. Blade lag dynamics are neglected, a linear lift aerodynamic model is used for the blade sections and approximate closed form expressions for the main rotor total hub aerodynamic loads are utilized. The model follows

Ref. [23] but uses a hinge offset representation rather than a center spring model. The dynamic inflow model used is that of Pitt-Peters [24].

Same as the load, the helicopter model is implemented as a state space model. The 21 element state vector of the helicopter, $\mathbf{x_H}$, is comprised of a 12 element rigid body state vector, $\mathbf{x_F}$, and a 9 element main rotor state vector, $\mathbf{x_R}$, as follows:

$$\mathbf{x_F} = \{u_H, v_H, w_H, p_H, q_H, r_H, \psi_H, \theta_H, \phi_H \; x_H, y_H, z_H\} \tag{3.a}$$

$$\mathbf{x_R} = \{\beta_0, \beta_{1S}, \beta_{1C}, \dot{\beta}_0, \dot{\beta}_{1S}, \dot{\beta}_{1C}, \lambda_0, \lambda_{1S}, \lambda_{1C}\} \tag{3.b}$$

$$\mathbf{x_H} = \{\mathbf{x}_F, \mathbf{x}_R\} \tag{3.c}$$

Similar to the load, the angular rates and inertial velocities of the helicopter are given in a fuselage fixed coordinate system (H) located at the helicopter center of gravity. The helicopter position vector is given in the earth fixed coordinate system (E). The transformation from (E) to (H) follows the conventional order of yaw, pitch, and roll Euler angles, ψ_H, θ_H, ϕ_H. The state vector of the main rotor includes the first harmonic flapping angles of the tip path plane and their rates of change, and the main rotor dynamic inflow components. The tail rotor is modeled using simplified closed form expressions for the force and moment coefficients.

The helicopter model includes a dynamic inversion (DI) control system consisting of an outer loop trajectory following model and an inner loop attitude and vertical speed control. The outer loop is designed to follow a desired reference trajectory, $\mathbf{u}$, defined by the combination of the vector of inertial velocity (u_N, v_E, w_D) in the earth fixed coordinate system and the flight heading (χ):

$$\mathbf{u} = \{u_N, v_E, w_D, \chi\} \tag{4}$$

The inner loop then uses a dynamic inversion of a piecewise reduced order linear model of the helicopter to produce the vector of control commands, $\boldsymbol{\delta}$. This vector includes the set of cyclic pitch, collective pitch and tail rotor pitch commands required to follow the desired trajectory:

$$\boldsymbol{\delta} = \{X_A, X_B, X_C, X_P\} \tag{5}$$

The DI controller does not include any compensation for the presence of the external load. A schematic of the helicopter control system is presented in Fig. 2. As the DI controller provides the desired stability and control characteristics for the helicopter, the stability augmentation system (SAS) of the UH-60 Black Hawk was not included in the model.

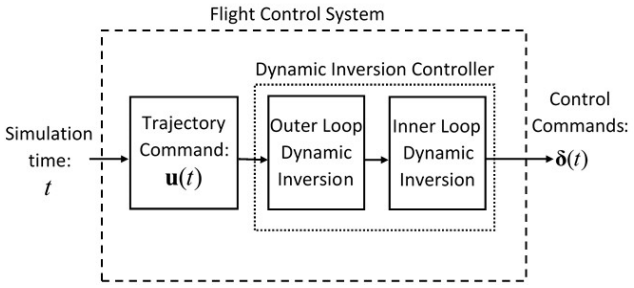

Fig. 2. Helicopter flight control system model

2.4. Active Cargo Hook

For the purposes of the current study, it was assumed that the cargo hook can move longitudinally and laterally relative to the helicopter, and is fixed in the vertical direction. The movement of the cargo hook relative to the helicopter following the actuation is expressed in the helicopter fixed coordinate system, H:

$$\Delta\mathbf{r_{CH}} = \Delta x_{CH} \cdot \hat{\mathbf{x}}_H + \Delta y_{CH} \cdot \hat{\mathbf{y}}_H \tag{6}$$

The active cargo hook actuators were modeled as a linear first order system with a cutoff frequency of 5 Hz. An actuator stroke limit of 4 ft was used with a maximal assumed stroke rate of 3 ft/s. During simulation, the actuator movement is controlled by the full state LQR controller, which will be described later. The term “full state“ denotes the use of all of the load states in the ACH controller, which was designed using an isolated load in a wind tunnel model. As will be shown later, for the coupled helicopter-external load system the controller actually uses relative states, i.e. the difference between the load states and the helicopter rigid body states.

2.5. Coupled Helicopter-External Load System

The equations of motion for the coupled system are assembled by combining the helicopter and load equations of motion with the controlled active cargo hook model:

$$\begin{bmatrix} \dot{\mathbf{x}}_\mathbf{L} \\ \dot{\mathbf{x}}_\mathbf{H} \\ \Delta\dot{\mathbf{r}}_\mathbf{CH} \end{bmatrix} = \begin{bmatrix} \mathbf{F_L}(\mathbf{x_L}, \mathbf{x_F}, \Delta\mathbf{r_{CH}}) \\ \mathbf{F_H}(\mathbf{x_L}, \mathbf{x_H}, \Delta\mathbf{r_{CH}}, \mathbf{u}) \\ \mathbf{G_{CH}}(\mathbf{x_L}, \mathbf{x_F}, \Delta\mathbf{r_{CH}}) \end{bmatrix} \tag{7}$$

In the equations above, $\mathbf{F_H}$ and $\mathbf{F_L}$ are the corresponding function vectors expressing the force and moment equations of the helicopter and the load, and $\mathbf{G_{CH}}$ is the dynamic model of the controlled cargo hook including the controller and actuator models. As a full-state feedback controller is used, it is assumed that all of the load states and all of the

helicopter rigid body states are available for the controller. The motion of the cargo hook induces changes in the sling cable forces as well as their arm relative to the center of gravity of the helicopter. Therefore, the cable hook states are included in the right-hand side of the helicopter and load equations of motion.

Two simulation models were developed in MATLAB/SIMULINK for use during controller development and performance validation. A model simulating an isolated load in a wind tunnel was first used for development of the LQR controller and evaluation of its effectiveness throughout the target airspeed envelope. A coupled model of the helicopter and external slung load was then used for validation of the controller efficiency in providing slung load stability during carriage by the helicopter. Figure 3 shows a schematic of the complete simulated system. It can be seen that the displacement of the active cargo hook, $\Delta\mathbf{r}_{\mathbf{CH}}$, is defined relative to the position of the fixed cargo hook that is normally mounted on the helicopter.

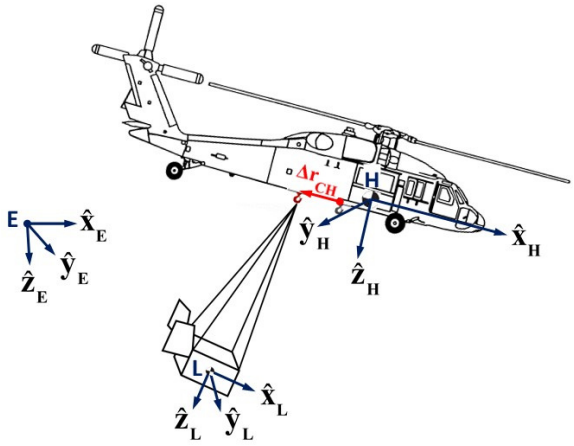

Fig. 3. Coupled helicopter-external load system

3. NONLINEAR DYNAMIC CHARACTERISTICS OF THE ISOLATED LOAD

The study of the isolated load dynamics was performed for a fixed cargo hook where the load is assumed to be mounted in a wind tunnel. With a fixed cargo hook, the equations of motion of the isolated load are expressed as an autonomous system (time not explicitly appearing in the equations) of the following form:

$$\dot{\mathbf{x}}_{\mathbf{L}} = \mathbf{F}_{\mathbf{W}}(\mathbf{x}_{\mathbf{L}}, V) \tag{8}$$

where V is the wind tunnel speed and $\mathbf{F}_{\mathbf{W}}$ is the function vector of the force and moment equations in this case. Note that using this mathematical formulation allows for the study of the system dynamics as a function of the airspeed (wind tunnel speed), V, which is treated as a parameter of the system.

The dynamic analysis of the system was performed using continuation and bifurcation tools of Dynamical Systems Theory (DST). For the analysis, the wind tunnel speed was used as the continuation parameter. The use of DST provides a comprehensive approach for the description of the slung load dynamics so that load stability can be efficiently evaluated for the entire relevant airspeed range of interest. The dynamic characteristics of the system are determined through the study of equilibria, solution trajectories, solutions periodicity and transition to chaos [25-27]. This approach had been applied before for the analysis of the fins stabilized CONEX and showed excellent agreement with wind tunnel test results [20]. In the current study, the continuation and bifurcation analysis was performed using the Dynamical Systems Toolbox [28], which is an integration of the continuation software package AUTO [29] into MATLAB.

Figure 4 presents the bifurcation curve for the load roll angle, ϕ_L, in equilibrium (trim) as a function of the wind tunnel speed. The terms “equilibrium” and “trim” will be used interchangeably next. The respective local stability of equilibrium points is noted by a solid blue line for stable solutions and dashed red lines for unstable solutions. The purple pentagrams denote pairs of Hopf bifurcation points, in between which limit cycle oscillations (LCO) exist. Further details can be found in Ref. [20].

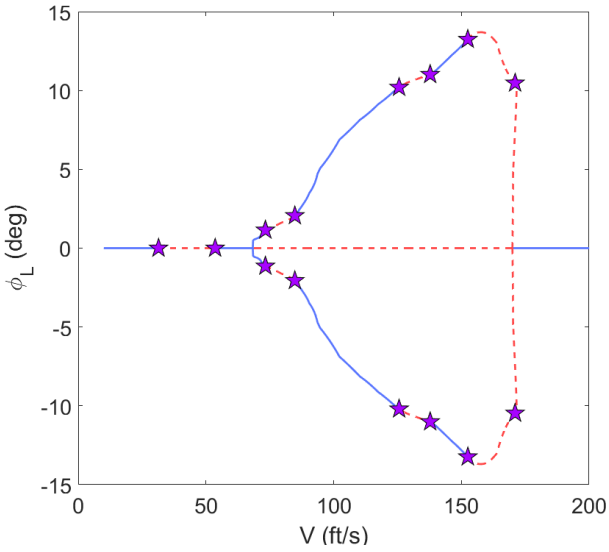

Fig. 4. Bifurcation curve of load roll angle

The bifurcation curve shows that at low speeds (up to 68 ft/s) and high speeds (above 170 ft/s), only a single solution branch exists, which corresponds to a symmetric equilibrium. In these airspeed ranges the

roll and yaw angles are both zero so that the load is pointing into the incoming flow with no sideslip. The solutions are stable for airspeeds well outside the region bounded by the two Hopf points at 30 ft/s and 54 ft/s and are periodic for airspeeds within or adjacent to this region. In the middle range (68 ft/s to 170 ft/s) three solution branches coexist. The symmetric branch for zero yaw and roll angles is unstable, and the other two asymmetric branches are either stable or include sub regions bounded by Hopf points couples, indicating periodic solutions. The instability of the center branch indicates that trajectory solutions are rejected away from it and attracted by the asymmetric branches, resulting either in load steady state trims at a nonzero sideslip angle, or a sustained periodic motion (LCO) about one of these branches. In many cases, sustained LCO solutions can extend beyond the airspeed range bounded by their respective Hopf bifurcation points.

At the design point airspeed of 100 kt (168.8 ft/s), three unstable equilibria exist: a symmetric equilibrium with ϕ_L=0 deg and two asymmetric equilibria with ϕ_L = ±10.9 deg. Solution trajectories for this point are characterized by sustained LCO. Figure 5 shows the trajectory time histories of the simulated system at 100 kt. An initial excitation is applied to the load 2 seconds into the simulation through a doublet in the lateral cargo hook position, otherwise kept fixed. The load yaw, pitch and roll angles time plots show two distinct LCO patterns: a symmetric LCO about the center solution branch (blue solid line) and an asymmetric LCO about the asymmetric branches (dashed black lines). The intensity of the excitation doublet determines which of the two trajectories is taken. Note that in the actual physical system, the trajectories may shift between the two solutions due to external disturbances such as atmospheric turbulence.

The coexistence of multiple solutions (equilibria and LCO) for the same airspeed is the direct result of the system nonlinearity. This complicates the design process of the LQR controller, which is essentially done using linear tools.

4. LQR CONTROLLER DESIGN

The design of the LQR controller was performed by obtaining approximate linear models for the system using linearizations about equilibria. Engineering judgment should be exercised during decision on the trim point used for the design. Both the symmetric and asymmetric equilibria can be chosen as trim points for linearization. However, the pole map of the linearized system (Fig. 6) shows that the unstable complex conjugate poles related to the LCO (0.048±j1.281rad/s) are present only when linearizing about the asymmetric solution branch. The real unstable pole of the symmetric branch at 0.51 rad/s corresponds to the divergence of the load away from the symmetric solution branch, once disturbed. This can be seen in the first few seconds of the initial time response presented in Fig. 5. Therefore, the linear approximation corresponding to an asymmetric trim point was used for controller design for the target airspeed of 100 kt.

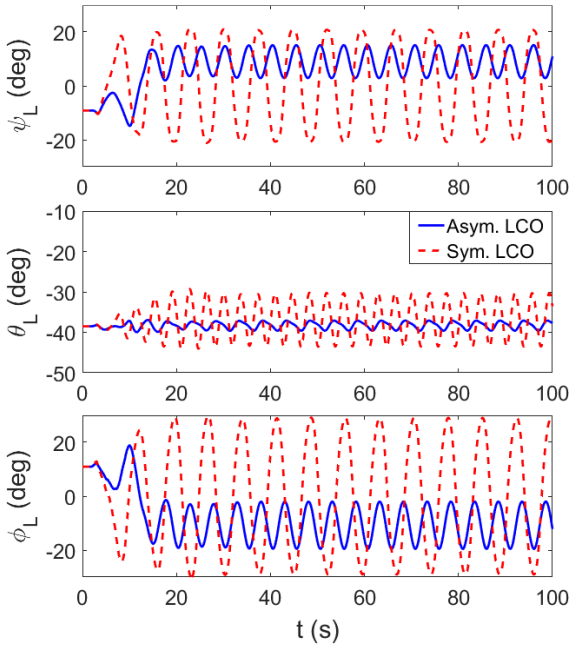

Fig. 5. Solution trajectories, 100 kt (168.8 ft/s)

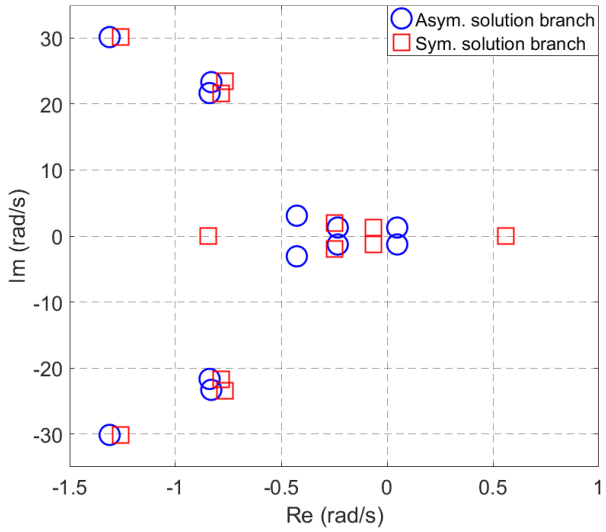

Fig. 6. Pole map, 100 kt (168.8 ft/s)

5. ACTIVE CARGO HOOK CONTROLLER DESIGN

Owing to the high level of dynamic coupling between

the longitudinal, lateral and directional planes of motions it was decided to design a full-state feedback linear quadratic regulator. This was further supported by the results obtained in an initial feasibility study using a simple roll angle proportional controller. The results showed that although the simple controller provided stability to the system, damping levels achieved were low. In addition, the controller failed to provide a complete decay of the oscillations in some cases.

A linear time invariant (LTI) model for the actuated isolated load was extracted from the nonlinear SIMULINK model by using the longitudinal and lateral positions of the cargo hook ($\Delta x_{CH}, \Delta y_{CH}$) as the inputs to the system, and the full 12 element load state vector ($\mathbf{x_L}$) as the system output. A first order actuator model was then added to the system to reflect the longitudinal and lateral actuators dynamics. The resulting state-space model of the linearized actuated system is given below:

$$\begin{aligned} \dot{\mathbf{x}}_\mathbf{A} &= \mathbf{A}_\mathbf{A} \cdot \mathbf{x}_\mathbf{A} + \mathbf{B}_\mathbf{A} \cdot \mathbf{u}_\mathbf{A} \\ \mathbf{y}_\mathbf{A} &= \mathbf{C} \cdot \mathbf{x}_\mathbf{A} + \mathbf{D} \cdot \mathbf{u}_\mathbf{A} \end{aligned} \tag{9.a}$$

with

$$\mathbf{x}_\mathbf{A} = \begin{bmatrix} \mathbf{x_L} \\ \Delta x_{CH} \\ \Delta y_{CH} \end{bmatrix}, \ \mathbf{u}_\mathbf{A} = \begin{bmatrix} \Delta x_{CH_{cmd}} \\ \Delta y_{CH\,cmd} \end{bmatrix},$$

$$\mathbf{A}_\mathbf{A} = \begin{bmatrix} \mathbf{A} & \mathbf{B} \\ \mathbf{0} & \begin{matrix} -\omega_A & 0 \\ 0 & -\omega_A \end{matrix} \end{bmatrix}, \ \mathbf{B}_\mathbf{A} = \begin{bmatrix} \mathbf{0} \\ \begin{matrix} \omega_A & 0 \\ 0 & \omega_A \end{matrix} \end{bmatrix}, \tag{9.b}$$

$$\mathbf{C}_\mathbf{A} = \mathbf{I}, \ \mathbf{D}_\mathbf{A} = \mathbf{0}$$

In equation (9.b) above, the system and control matrices (**A**,**B**) are those of the isolated load model without the actuation dynamics. ω_A is the actuator cutoff frequency of 31.4 rad/s (5 Hz). It should also be noted that the linear model presented in eqns (9) is a small perturbation model of the system so that the vectors $\mathbf{x}_\mathbf{A}$ and $\mathbf{u}_\mathbf{A}$ are actually the perturbed states and controls.

The LQR controller design was obtained by using full-state feedback of the form:

$$\mathbf{u}_\mathbf{A} = -\mathbf{K} \cdot \mathbf{x}_\mathbf{A} \tag{10}$$

The LQR feedback gain matrix, **K**, was obtained by numerical solution of the algebraic Riccati equation:

$$\mathbf{A}_\mathbf{A}^T \cdot \mathbf{P} + \mathbf{P} \cdot \mathbf{A}_\mathbf{A} + \mathbf{Q} - \mathbf{P} \cdot \mathbf{B}_\mathbf{A} \cdot \mathbf{R}_\mathbf{A}^{-1} \cdot \mathbf{B}_\mathbf{A}^T \cdot \mathbf{P} = \mathbf{0} \tag{11.a}$$

$$\mathbf{K} = \mathbf{R}^{-1} \cdot \mathbf{B}_\mathbf{A}^T \cdot \mathbf{P} \tag{11.b}$$

The state and control weight matrices **Q** and **R** were chosen using a trial and error approach. As will be shown later, these set values provided good stabilization capabilities for an airspeed of 100 kt, but had to be modified at a later stage in order to provide stabilization across the target airspeed envelope:

$$\begin{aligned} \mathbf{Q} &= 33 \cdot \mathrm{diag}\left(\left[0,0,0,1,1,1,1,1,1,0,0,0,0,0\right]\right) \\ \mathbf{R} &= \mathrm{diag}\left(\left[1,1\right]\right) \end{aligned} \tag{12}$$

The state weight matrix **Q** used equal weights on the load attitudes and angular rates, and zero weights for the load velocities and positions. Because of the relative high stiffness of the sling cables, their lengths remain approximately constant following the initial stretch due to the load weight. This implies that the velocity and position of the load center of gravity can be approximately expressed as direct algebraic functions of the attitudes and angular rates. Therefore, their influence in **Q** would be similar to that of the attitude and rate terms and hence is redundant.

The full-state feedback control law in eqn (10) uses the perturbed state vector for the calculation of the actuator control command. The perturbed state vector is defined as the difference between the instantaneous state vector and its equilibrium value, which is unknown. By passing the instantaneous state vector through a low pass filter, an approximate value for the trim state vector can be obtained. A schematic of the full-state feedback controller and actuation system of the active cargo hook is presented in figure 7.

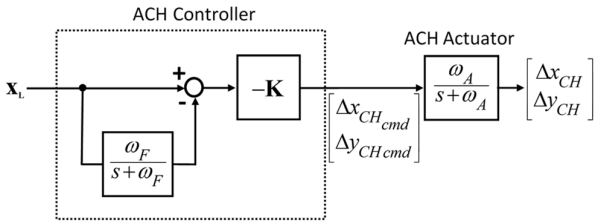

Fig. 7. Active cargo hook LQR controller and actuator models

Figure 8 shows the time response of the controlled system for an airspeed of 100 kt. For comparison, the trajectories are overlaid over the time response of the uncontrolled system with symmetric LCO, presented earlier in Fig. 5. The load is initially at an asymmetric equilibrium point. The system is then excited by applying initial longitudinal and lateral velocities of 12 ft/s to the load. This simulated "push" of the load is the technique most frequently used during dynamic wind tunnel tests to excite the system. During the initial transitory response, the load develops large attitude angles. However, the controller swiftly returns the load back towards equilibrium. Within 20 s of the excitation, the load is back at rest in its initial

asymmetric equilibrium point. Figure 9 shows the corresponding longitudinal and lateral strokes of the active cargo hook during the simulation. Over the first five seconds of the simulation, the system tries to fight the large attitude angles and angular rates that develop following the initial push of the load. It can be seen that both the longitudinal and lateral actuators are saturated reaching their physical stroke limit of 4 ft. In addition, the stroke rate limit of 3 ft/s is also reached as can be seen by the constant gradients of the curves during this period. This relatively short time where the actuators are saturated does not prevent the controller from stabilizing the load. As can be observed, the abrupt response of the active cargo hook to the initial fast movement of the load brings the load close to its equilibrium position. From here on, the controller is using mild actuation commands to return the load back to equilibrium, which is quickly reached.

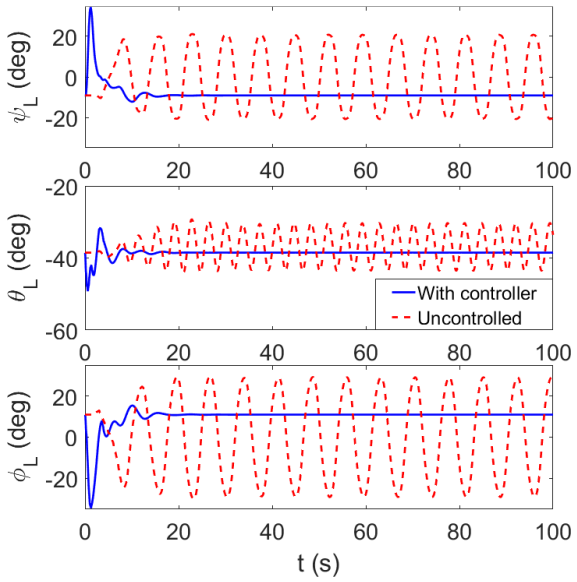

Fig. 8. Solution trajectories of the controlled and uncontrolled systems, 100 kt (168.8 ft/s)

Another demonstration of the controller performance is provided in Fig. 10. In this case, the controller is switched on only 40 s into the simulation, after significant oscillations have already developed. Here again, a reference case for an uncontrolled system is also included. This maneuver simulates a situation where the system would be normally off during flight and switched on only when oscillations are encountered. As can be observed, the controller does a good job in eliminating the oscillations and returning the system to equilibrium. The maximal cargo hook displacements encountered for this case (not shown)

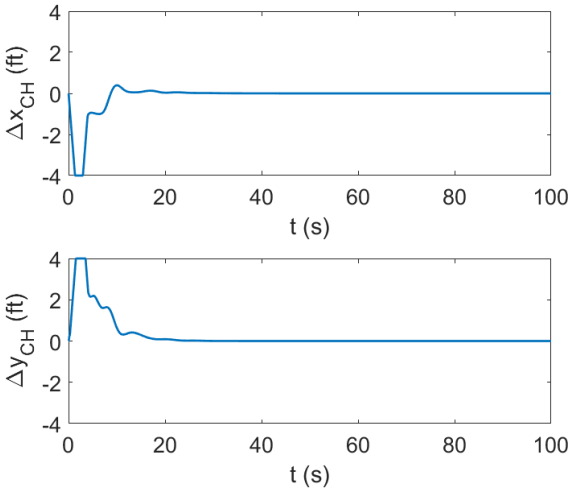

Fig. 9. Cargo hook displacement following load excitation, 100 kt (168.8 ft/s)

were 53% of the maximum physical limit. Stroke rate saturation occurred only once, during the first second after controller switch-on.

Additional simulations were run for various combinations of initial conditions. The results showed that the current controller design is robust as no load instabilities were found for the 100 kt point. This showed that the current design approach is feasible for providing load stabilization. Following this conclusion, the design process was now applied for the entire target airspeed envelope. Gain matrices were calculated by solving the Riccati equation for airspeeds between hover (5 kt) and 140 kt in 5 kt increments. The validation of the controller performance throughout this target envelope is described next in the “results” section.

6. RESULTS

6.1. Controller Performance Validation

The validation of the controller performance was achieved using a Monte-Carlo algorithm, which was used for drawing different sets of perturbations in the longitudinal and lateral speed components of the load. These were then used as initial conditions for the simulation of the isolated load. The results showed that the controller design is successful in stabilizing the load in most parts of the target airspeed envelope. The controller failed to provide stabilization in the following airspeed ranges: 75 kt to 80 kt (126.6 ft/s to 135 ft/s) and above an airspeed of 100 kt (168.8 ft/s). Also, LCO or very low damping were observed around an airspeed of 40 kt (67.5 ft/s). The nonlinear dynamic analysis shows that in these areas large LCO amplitudes are expected to exist for the uncontrolled system. This can also be observed by the bifurcation curve (Fig. 4) for the two higher airspeed regions, which are within/partly within the

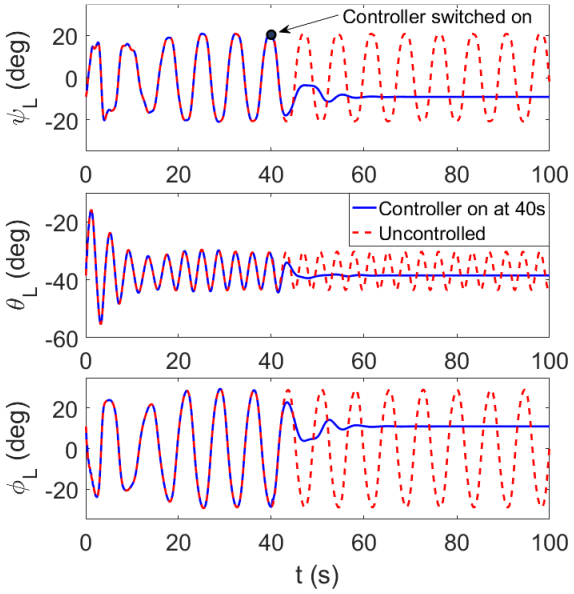

Fig. 10. Solution trajectories following controller switch on at 40 s, 100 kt (168.8 ft/s)

range bounded between two Hopf bifurcation points. The lower airspeed of 40 kt is outside the range of 18.5 kt to 32 kt (31.4 ft/s to 53.6 ft/s) bounded by the two adjacent Hopf bifurcation points and is therefore expected to be stable. However, nonlinear dynamic analysis shows that the oscillations in this range are subcritical so that the oscillations "spill over" beyond the bounding Hopf points.

In order to correct these deficiencies the constant weight matrices were replaced by airspeed scheduled weights to account for the different contributing factors for the oscillations still occurring in the controlled system. In the low airspeed range where the aerodynamic loads are low, LCO damping was increased by reducing the control weight matrix, **R**. This allowed the controller to use larger cargo hook strokes in order to respond to the oscillations. In the high airspeed range, the aerodynamic damping provided by the fins is high due to the higher dynamic pressure. In addition, the LCO amplitude is much higher as compared to that of the low airspeed range. In this airspeed range the angular rate terms in the state weight matrix were set to zero to eliminate the added damping of the controller. In addition, the weights of the attitude states were significantly increased to make the controller more abrupt, and limit the load from maintaining the large attitude angles that were used as the initial conditions in the simulations resulting in the symmetric high amplitude LCO. The modified weight matrices are received by multiplying the original matrices **Q** and **R**, by respective airspeed scaling functions, $f_{\mathbf{Q}}(V)$ and $f_{\mathbf{R}}(V)$. The scaling ratios for the attitude and angular rate terms in **Q** and the control terms in **R** are shown in Fig. 11.

Figures 12 and 13 show the attitude time response and corresponding cargo hook displacement for the original and modified gain set at an airspeed of 75 kt (126.6 ft/s). The trajectory of the uncontrolled system is also included for comparison. Figure 12 shows that the original controller design actually makes the oscillations more severe. While the uncontrolled system shows a mild asymmetric oscillation with a roll angle amplitude of 1.8 deg, the original controller gains excite the more violent symmetric oscillations having a significantly larger amplitude of 28.2 deg. With the modified gains, the system quickly returns to equilibrium following the initial excitation.

The cargo hook stroke curves presented in Fig. 13 show that with the original controller, the longitudinal hook position is rate saturated all the time, and keeps

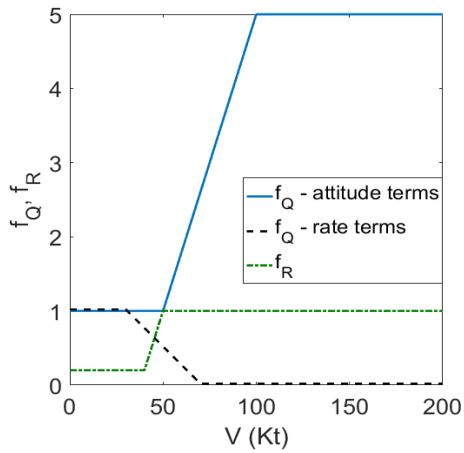

Fig. 11. Airspeed scaling of weight matrices

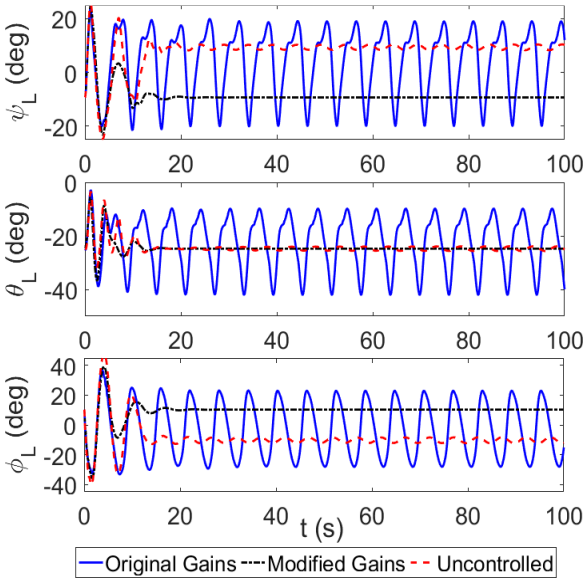

Fig. 12. Effect of gain modification, 75 kt (126.6 ft/s)

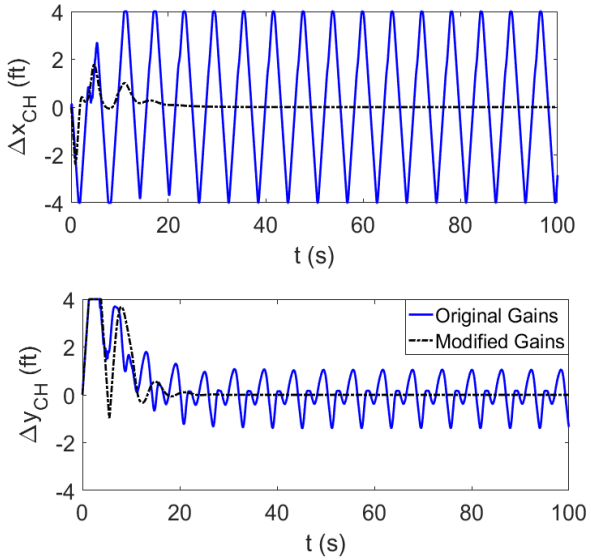

Fig. 13. Cargo hook stroke, 75 kt (126.6 ft/s)

bouncing between the physical displacement limits. Interestingly, the rate saturation in the lateral direction is present only part of the time. This is expected as the frequency of the longitudinal oscillation is twice that of the lateral oscillation, so that the controller has to work twice as fast to overcome it. With the modified gains, the system is swiftly controlled, with a single saturation of the actuator following the initial excitation of the load.

Simulations with the modified controller design showed that most of the deficiencies identified were resolved by the improved design. A very small instability region about an airspeed of 101 kt (170.5 ft/s) remained even with the modified design and is an inherent characteristic of the nonlinear system. Figure 14 shows a close-up of the bifurcation curve about this airspeed. The dashed arrows follow the system trajectory during the oscillations. Due to the incremental induced airspeed by the lateral pendulum motions, the load total airspeed is oscillating. When the load moves inboard toward the centerline, the airspeed increases. The trajectory first follows the asymmetric branch, until the airspeed increases beyond that of the fold point at 101.7 kt (171.7 ft/s) on the bifurcation curve, where the trajectory "falls off" the asymmetric branch and starts following the symmetric branch. As the load moves past the centerline, its airspeed starts to decrease. The load first moves back along the symmetric bifurcation branch until it reaches the branch point at 100.7 kt (170 ft/s), where it jumps back to the asymmetric branch. Figure 15 presents the respective trajectory at 101 kt. The initial response shows that the load hesitates between the two LCO solutions until settling into what appears as symmetric LCO. However, a closer examination of the curves shows that the oscillations are not exactly symmetric, a result of the load going into and out off the attraction zones of the symmetric and asymmetric solution branches. This complicated pattern creates an hysteresis effect that is difficult to control. Due to the problem being confined to a negligible part of the envelope it was decided not to pursue this anomaly further. Moreover, once coupled to the helicopter, the added oscillation damping provided by the main rotor resulted in the system being stable also at 101 kt.

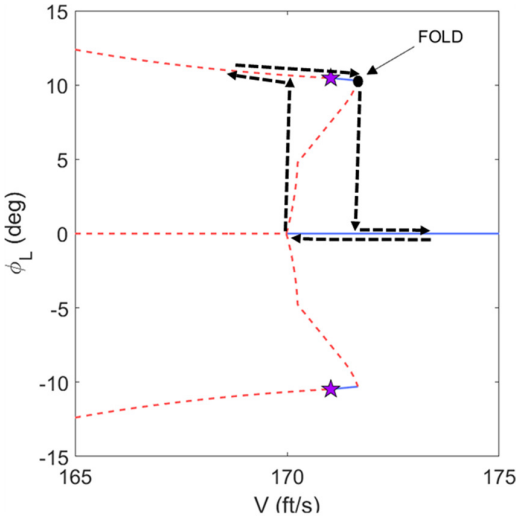

Fig. 14. Controlled system instability near fold, 101 kt (170.5 ft/s)

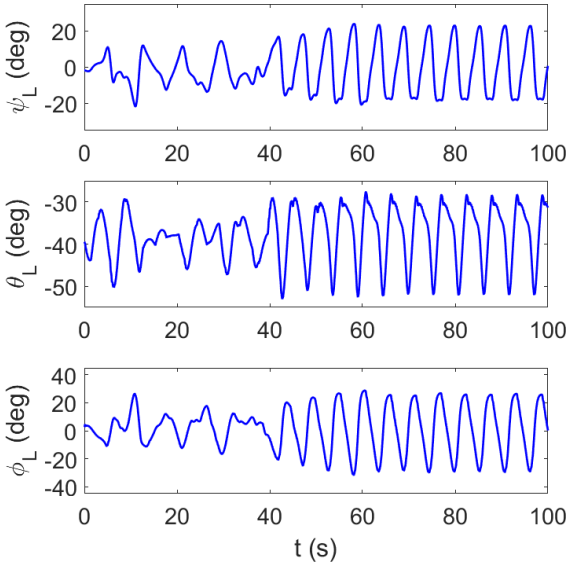

Fig. 15. Controlled system trajectory, 101 kt (170.5 ft/s)

6.2. Controller Design and Performance for the Coupled Helicopter-Slung Load System

As explained earlier, the development of the ACH controller was achieved using a model of an isolated load in a wind tunnel. This essentially means that the

equilibrium position of the load is fixed in space and that the equilibrium inertial velocity of the load is zero. During forward flight, these conditions change so that the equilibrium position of the load is fixed relative to the helicopter, and its inertial velocity is identical to the helicopter velocity. Therefore, the load position and velocity input signals to the full state feedback controller were now replaced by their respective values relative to the helicopter. In order to maintain unity, the load absolute attitude and angular rate signals feeding into the ACH controller were also replaced by their respective magnitudes relative to the helicopter. However, simulations showed that this had only a small effect on the controlled system.

Flight tests have shown that the coupling between the helicopter and the load introduces additional damping into the system [30]. This is because when carried by a helicopter, some of the load energy was dissipated by the free stream flow through aerodynamic damping of the helicopter rotors. Simulations of the coupled system that were run at the design airspeed of 100 kt showed that due to the phenomenon described above, the system turned stable even without the ACH controller. For this reason, controller performance for the coupled helicopter-slung load system is demonstrated for an airspeed of 97 kt (163.8 ft/s), where the coupled system without the ACH controller is still unstable.

Simulation results for the system with and without the ACH are presented in Figs. 16-18 that show the attitude time history of the helicopter and load, and the ACH stroke. In this case, the system was excited by applying a lateral control doublet through the helicopter DI controller. This was done by commanding a lateral velocity doublet of 10 ft/s 5 seconds into the simulation. The results show the coupling between the helicopter and the load. Without the ACH, the load roll angle amplitude of 29 deg induces coupled roll/yaw oscillations in the helicopter that result in the pilots experiencing oscillatory lateral load factors in the order of 0.2 g. Although not an immediate safety of flight concern, flight in presence of this high level of oscillations significantly increases pilot workload and decreases the ride quality. Therefore, flight in such conditions can be maintained by the aircrew only for a short period of time. When the ACH is present, the load oscillations quickly die out following the roll doublet. Because the controller guarantees system stability, any transient oscillations excited by turbulence will quickly damp out so that positive system stability will be maintained and pilot workload will not be affected. Figure 18 shows that although the ACH appears to be rate saturated during its initial response to the roll doublet, it has no difficulty in damping out the load motion. As the roll doublet is severe, resulting in a helicopter bank to bank roll angle change of 25.5 deg, these results demonstrate the benefit of the inclusion of an active

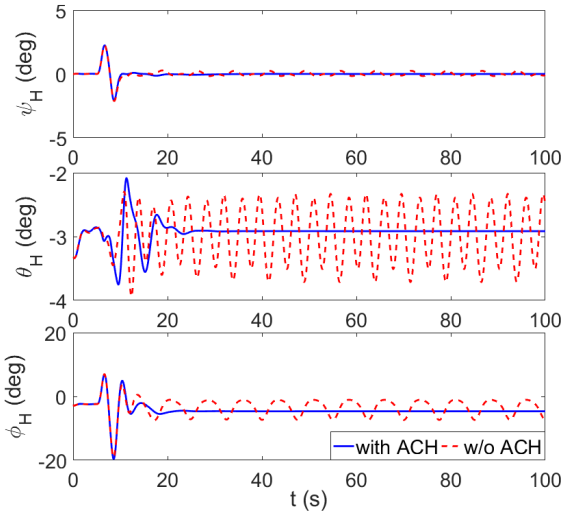

Fig. 16. Helicopter attitude, 97 kt (163.8 ft/s)

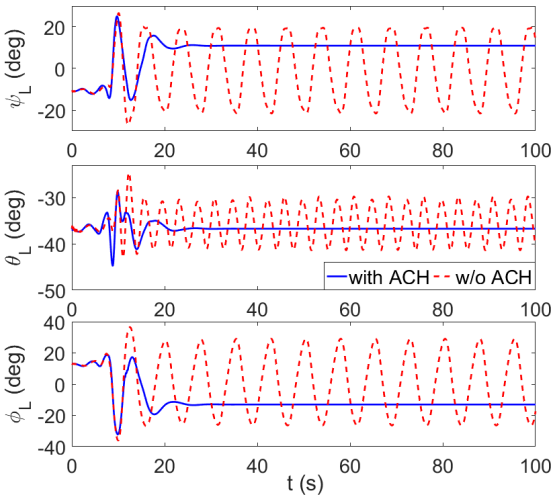

Fig. 17. Load attitude, 97 kt (163.8 ft/s)

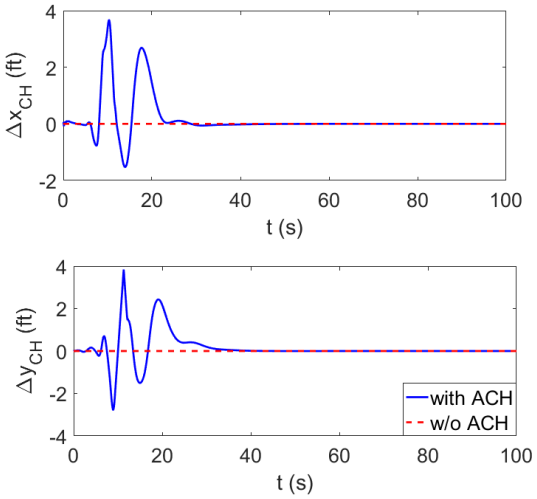

Fig. 18. Cargo hook stroke, 97 kt (163.8 ft/s)

cargo hook system in the helicopter.

As a further validation of the ACH controller performance, a complex maneuver was simulated. The maneuver is composed of the following basic mission segments: level acceleration, cruise (straight and level flight), level right turn and climb. The cruise, turn and climb segments were all performed at a constant airspeed of 97 kt (163.7 ft/s). The rate of climb for the climb segment was set to 25 ft/s. The simulation started from a trimmed hover out of ground effect (OGE) with the helicopter facing north. Table 1 details the maneuver segments and the corresponding start and end times for each segment.

Table 1. Maneuver segments

No.	Maneuver segment	Start time [s]	End time [s]
1	Trimmed hover OGE	0	1
2	Level acceleration	1	21
3	Level cruise	21	51
4	Leve right turn to the east	51	71
5	Level cruise	71	101
6	Climb, rate of climb 25 ft/s	101	121
7	Level cruise	121	150

Time plots of the helicopter and load attitude angles are shown in Figs. 19 and 20, respectively. The plots include results for the system with and without the active cargo hook. For clarity, vertical dashed lines were included in the figures as separators between the different maneuver segments. Referring to Fig. 19, the effect of the ACH is apparent in the helicopter pitch and roll angles. While sustained oscillations are clearly visible when the ACH is not present, these either disappear altogether or show positive damping when the ACH is included in the system. The oscillations are most apparent in the cruise sections, and reduce during the turn and climb segments. The change of load factor in these segments is equivalent to a change in the load weight, leading to modified load dynamics and oscillation pattern. As indicated earlier, although the oscillations in the absence of the ACH system do not appear large, they induce significant lateral accelerations at the cockpit that are objectionable to the pilots. Figure 20 reiterates the effectiveness of the ACH because of the significant level of load oscillations present with its absence. The most apparent difference can be observed in the cruise segments, where the load settles into large symmetric oscillations when the ACH is not included in the system. With the ACH, no load oscillations are observed during most maneuver segments. Small

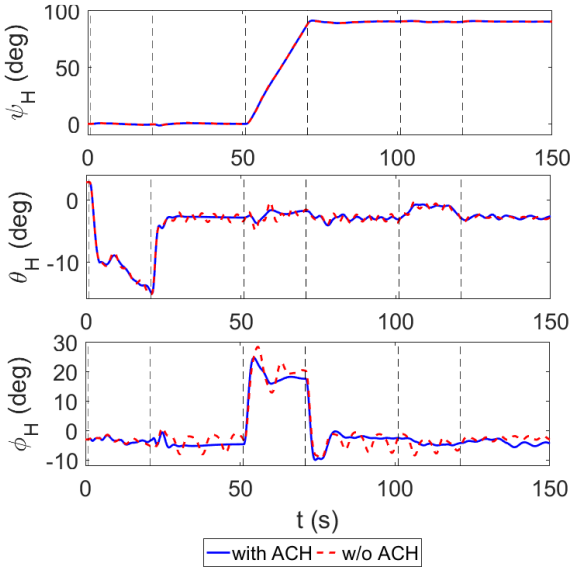

Fig. 19. Helicopter attitude angle during a complex maneuver

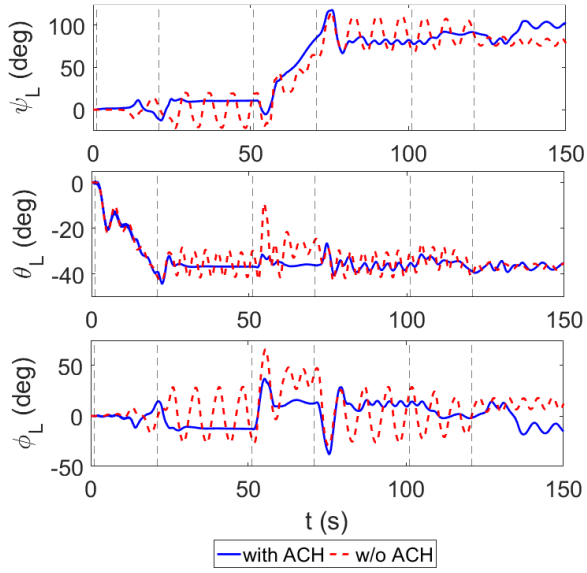

Fig. 20. Load attitude angle during a complex maneuver

asymmetric oscillations can be observed in the second and last cruise segments. These have low amplitudes and a positive low damping ratio of 0.02. During the design of the controller, the main objective was to keep the high-intensity symmetric LCO damped. This required a design compromise to be made during the gain selection with regard to the damping of the mild asymmetric LCO at a limited range of airspeeds. As can be observed in Fig. 19, the resulting oscillations in the helicopter are small. The damping ratio of the asymmetric oscillations can be improved by fine tuning the LQR controller gains

about the 97 kt point through modification in the state and control weight matrices, **Q** and **R**.

7. CONCLUSIONS

An active cargo hook system is effective in stabilizing external loads during high speed flight. The use of a full-state feedback linear quadratic regulator for controlling the active cargo hook was found to be a proper approach. However, as the design process relied on linear approximations of a nonlinear system, a nonlinear dynamic analysis of the baseline system dynamics prior to controller design was essential. Further, the familiarity with the nonlinear dynamic characteristics of the system as a function of airspeed facilitated the process of setting the controller gain schedule. The incorporation of a control actuated cargo hook in the helicopter provided stable flight throughout the airspeed envelope with a minimal level of system oscillations. Carriage of problematic external loads, that is currently limited to low airspeeds due to stability or handling qualities issues can likely be extended by use of such system, with a significant improvement in operational effectiveness.

8. ACKNOWLEDGMENTS

This research was partially funded by the Government under Agreement No. W911W6-17-2-0003. The U.S. Government is authorized to reproduce and distribute reprints for Government purposes notwithstanding any copyright notation thereon. The views and conclusions contained in this document are those of the authors and should not be interpreted as representing the official policies, either expressed or implied, of the Aviation Development Directorate or the U.S Government.

REFERENCES

1. Sheldon, D. F., "Appreciation of Dynamic Problems Associated with External Transportation of Loads from a Helicopter-State of Art," *Vertica,* Vol. 1, (4), 1977, pp. 281-290.
2. Watkins, T. C., Sinacori, J. B., and Kesler, D. F., "Stabilization of externally slung helicopter loads [Final Report, 1 Jul. 1972 - 31 Oct. 1973]," USAAMRDL-TR-74-42, August 1974.
3. Liu, D. T., "In-Flight Stabilization of Externally Slung Helicopter Loads [Final Report, 25 Jun. 1970 - 17 Jun. 1972]," USAAMRDL Tech. Rept. 73-5, May 1973.
4. Asseo, S. J., and Whitbeck, R. F., "Control requirements for sling-load stabilization in heavy lift helicopters," *Journal of the American Helicopter Society,* Vol. 18, (3), July 1973, pp. 23-31.
5. Micale, E. C., and Poli, C., "Dynamics of slung bodies utilizing a rotating wheel for stability," *Journal of Aircraft,* Vol. 10, (12), 1973, pp. 760-763.
6. Feaster, L. L., "Dynamics of a Slung Load," PhD Thesis, Department of Mechanical and Aerospace Engineering, Massachusetts Univesity, Amherst, June 1975.
7. Pardue, M. D., and Shaughnessy, J. D., "Design and analysis of an active jet control system for helicopter sling loads," NASA TP 1397, January 1979.
8. Nagabhushan, B. L., "Optimal controller design for a helicopter using its lower order dynamic model," American Institute of Aeronautics and Astronautics, Aircraft Design, Systems and Technology Meeting, Fort Worth, TX, October 17-19, 1983.
9. Raz, R., Rosen, A., and Ronen, T., "Active Aerodynamic Stabilization of a Helicopter Sling-Load System," *Journal of Aircraft,* Vol. 26, (9), September 1989, pp. 822-828.
10. Ehlers, G. E., "Hi-Fidelity Simulation and Prediction of Helicopter Single Point External Load Stabilization," M.Sc. Thesis, Naval Postgraduate School, Monterey, California, September 2001.
11. Hamers, M., and Bouwer, G., "Flight director for helicopter with slung load," 30th European Rotorcraft Forum, Marseilles, France, September 14-16, 2004.
12. Hamers, M., and Bouwer, G., "Helicopter Slung Load Stabilization Using a Flight Director," American Helicopter Society International 60th Annual Forum, Grapevine, TX, June 1-3, 2005.
13. Hamers, M., "Flight director for handling of helicopter sling loads," 31st European Rotorcraft Forum, Florence, Italy, September 13-15, 2005.
14. Hamers, M., Von Hinuber, E., and Richter, A., "Flight director for slung load handling - First experiences on CH53," 33rd European Rotorcraft Forum, Kazan, Russia, September 11-13, 2007.
15. Raz, R., Rosen, A., Carmeli, A., Lusardi, J., Cicolani, L. S., and Robinson, D., "Wind tunnel and flight evaluation of passive stabilization of a cargo container slung load," *Journal of the American Helicopter Society,* Vol. 55, (3), July 2010, pp. 0320011-03200118.
16. Cicolani, L., Ivler, C., Ott, C., Raz, R., and Rosen, A., "Rotational stabilization of cargo container slung loads," American Helicopter Society International 69th Annual Forum, Alexandria, VA, May 21-23, 2013.
17. Ivler, C., "Design and Flight Test of a Cable Angle Feedback Control System for

Improving Helicopter Slung Load Operations At Low Speed," RDMR-AF-14-01, April 2014.
18. Krishnamurthi, J., and Horn, F. J., "Helicopter Slung Load Control Using Lagged Cable Angle Feedback," *Journal of the American Helicopter Society,* Vol. 60, (2), 2015, pp. 1-12.
19. Patterson, B. W., Enns, R., King, C., Kashawlic, B. E., Mohammed, S., and Lukes, G., "Design and Flight Test of a Hybrid External Load Stabilization System for an H-6 Helicopter Testbed," American Helicopter Society 71st Annual Forum, Virginia Beach, Virginia, May 5-7, 2015.
20. Enciu, K., and Rosen, A., "Nonlinear Dynamical Characteristics of Fin-Stabilized Underslung Loads," *AIAA Journal,* Vol. 53, (3), March 2015, pp. 723-738.
21. Enciu, K., and Rosen, A., "Aerodynamic Modeling of Fin Stabilized Underslung Loads," *Aeronautical Journal,* Vol. 119, (1219), September 2015, pp. 1073-1103.
22. Howlett, J. J., "UH-60A Black Hawk Engineering Simulation Program: Volume I – Mathematical Model," SER 70452 (NASA Contractor Report 166309), December 1981.
23. Padfield, G. D., *Helicopter Flight Dynamics: The Theory and Applications of Flying Qualities and Simulation Modelling*, AIAA Inc., Washington DC, 1966.
24. Pitt, D. M., and Peters, D. A., "Theoretical Prediction of Dynamic Inflow Derivatives," *Vertica,* Vol. 5, (1), pp. 21-34.
25. Nayfeh, A. H., and Balachandran, B., *Applied Nonlinear Dynamics: Analytical, Computational, and Experimental Methods*, Wiley-VCH Verlag GmbH & Co. KGaA, Weinheim, 1995.
26. Strogatz, S. H., *Nonlinear Dynamics And Chaos*, Perseus Books, Reading, 1994.
27. Wiggins, S., *Introduction to Applied Nonlinear Dynamical Systems and Chaos*, Springer, New York, 2003.
28. "Dynamical Systems Toolbox," Coetzee, E., 2011, http://www.mathworks.com/matlabcentral/fileexchange/32210-dynamical-systems-toolbox [retrieved 1 March, 2012].
29. "AUTO-07P, Software Package," Computational Mathematics and Visualization Laboratory, C. U., Montreal, Canada, 2007, http://indy.cs.concordia.ca/auto/ [retrieved 1 March, 2012].
30. Raz, R., Rosen, A., Cicolani, L. S., Lusardi, J., Gassaway, B., and Thompson, T., "Using wind tunnel tests for slung loads clearance," 67th American Helicopter Society International Annual Forum, Virginia Beach, VA, May 3-5, 2011.